RECENT DEVELOPMENTS IN RAIN-WIND INDUCED VIBRATIONS OF CABLES

Ian J Taylor [1], Andrew C Robertson [1],
Stephen K Wilson [2], Brian R Duffy [2], Julie M Sullivan [2]

[1] *Department of Mechanical Engineering, University of Strathclyde, Glasgow, G1 1XJ*

[2] *Department of Mathematics, University of Strathclyde, Glasgow, G1 1XH*

ABSTRACT :

On wet and windy days, the inclined cables of cable-stayed bridges can experience large amplitude, potentially damaging oscillations known as Rain-Wind Induced Vibration (RWIV). RWIV is believed to be the result of a complicated nonlinear interaction between rivulets of rain water that run down the cables and the wind loading on the cables from the unsteady aerodynamics; however, despite a considerable international research effort, the underlying physical mechanism that governs this oscillation is still not satisfactorily understood.

An International Workshop on Rain-Wind Induced Vibration was held in April 2008, hosted at the University of Strathclyde. The aim of this meeting was for a number of the key international researchers to discuss the latest research findings, establish key areas of uncertainty about the underlying physics for RWIV, and identify the most important directions for future research. The main outcomes of this workshop are summarised in the paper. Key themes of the Workshop included the exact role rivulets have in the oscillatory mechanism, the similarities between dry-inclined galloping and RWIV, the role of Karman vortex suppression on the instability, and the effect of the variation of the aerodynamic forces in the critical Reynolds number regime.

A numerical method to investigate aspects of the RWIV phenomenon has recently been developed by the authors, which couples an unsteady aerodynamic solver to a thin-film model based on lubrication theory for the flow of the rain water to ascertain the motion of the rivulets due to the unsteady aerodynamic field. This novel numerical technique, which is still in the relatively early stages of development, has already provided useful information on the

coupling between the external aerodynamic flow and the rivulet, and a summary of some of the key results to date is presented.

NOMENCLATURE

B	solid body in unsteady aerodynamic solver
C_D	coefficient of drag
$\overline{C}_D$	mean (time averaged) coefficient of drag
$\overline{C}_F^*$	normalised mean (time averaged) coefficient of friction
C_L	coefficient of lift
$\overline{C}_L$	mean (time averaged) coefficient of lift
$\overline{C}_P$	mean (time averaged) coefficient of pressure
F	flow field in unsteady aerodynamic solver
g	acceleration due to gravity
H, h	thickness of water film on surface of cylinder (normal to surface)
i, j, k	unit orthogonal vectors
n, *n*	unit vector and distance normal to body surface
P, p	pressure distribution
Q	azimuthal volume flux of fluid in the film
R	radius of cylinder
Re	Reynolds number $=\frac{UD}{\nu}$ where *D* is the cable diameter
r	position vector
r, θ, *z*	polar coordinates with the *z* axis along the axis of the cylinder and θ measure from upstream stagnation point
s, *s*	unit vector and distance tangential to body surface
S	surface of body in unsteady aerodynamic solver
T	shear distribution
t	time
U, **U**	velocity magnitude and vector
u, v	horizontal and vertical velocities
x, y	horizontal and vertical directions
α	cable inclination angle
β	cable yaw angle (angle of cable to wind direction)
γ	surface tension of water

ε (= H/R)	ratio of thickness of film to cylinder radius
ζ	damping ratio
θ	angle around circumference of cylinder from stagnation point
κ	mean curvature of the free surface of the film
μ	dynamic viscosity of fluid
ν	kinematic viscosity of fluid
ρ	density of fluid
$\boldsymbol{\Psi}$, Ψ	vector potential and stream function
Ω	rotational velocity of solid body
$\boldsymbol{\omega}$, ω	vorticity (vector and magnitude)

INTRODUCTION

On wet and windy days, the inclined cables of cable-stayed bridges can experience large amplitude oscillations known as Rain-Wind Induced Vibration (RWIV). Since the phenomenon was first reported by Hikami in 1988 (Hikami and Shiraishi, 1988), RWIV has been the focus of a considerable amount of research activity in the international wind- and bridge-engineering communities. Despite this research effort, a full understanding of the aeroelastic phenomenon has yet to be obtained due to the complexity of the interaction between the rivulets of rain water running down the inclined cable, the unsteady aerodynamic flow field, and the structural dynamics of the cable.

Data from full scale investigations and wind tunnel experiments undertaken since the original observation of Hikami and Shiraishi (1988) have provided a sizeable knowledge base concerning the conditions under which RWIV most commonly occurs. Notable examples of bridges on which RWIV have been investigated are the Erasmus Bridge, Rotterdam, The Netherlands (Geurts *et al*, 1998), the Fred Hartman Bridge, Baytown, Texas (Zuo *et al*, 2008), and the Dongting Lake Bridge, Hunan Province, China (Ni, *et al*, 2007).

In summary, this data suggests that RWIV tends to occur only over a restricted range of wind velocities, typically between 5 and 15 m/s (Table 1), under "moderate" rain conditions[†] for cables that descend in the direction of the wind ($0° < \beta < 180°$) in terms of the angles defined in Fig. 1. Cable inclination angles, α, are typically between 20° and 50°, and yaw angles, β, are typically between 20° and 50°. The cables themselves normally have diameters in the range 100 to 250mm, and have low structural damping ($\zeta \leq 0.5\%$), while the response is generally in the frequency range 0.6 to 3 Hz and normally occurs in

[†] A consistent definition of "moderate" rain cannot be obtained from the published research.

the cable-pylon plane (Fig. 1). Through such characteristics RWIV can be identified as a distinct aeroelastic phenomenon, with particular features that distinguish it from other aeroelastic instabilities such as galloping or vortex-induced vibration.

One of the key aspects of the RWIV instability is the presence and location of the rivulets of rain water on the surface of the cable. In experiments, it has been observed that the thin film of rain water present on the cable normally accumulates to form two rivulets near the separation points of the external aerodynamic field around a dry cable (Bosdogianni and Olivari, 1996). Other studies have concentrated on specific aspects of the location and dynamics of the rivulet motion, to identify the effect of the rivulets on the external aerodynamic field and vice versa. The latter investigations can be broadly separated into two distinct classes, namely those where the rivulet is replaced by a fixed, static, rigid protuberance, i.e. an 'artificial rivulet' (Matsumoto *et al*, 1995, Bosdogianni and Olivari, 1996) and those where a film of water is sprayed onto the surface of the cable and the rivulets are allowed to form 'naturally' (Flamand, 1995, Cosentino *et al*, 2003, Verwiebe and Ruscheweyh, 1998, Gu and Du, 2005, Wang *et al*, 2005). Both classes indicate that the presence of the rivulet on the upper surface is largely responsible for the vibration (Matsumoto *et al*, 1995), while the latter class also indicates that when free to do so, the rivulets oscillate circumferentially at the same frequency as that with which the cable vibrates. Differentiating between the effect of circumferential oscillation and rivulet position in the 'artificial rivulet' investigations has, however, proven more difficult and led to discrepancies in the literature. In particular Verwiebe and Ruscheweyh (1998) determined that the circumferential oscillation of the rivulet is a primary cause of RWIV, whereas Bosdogianni and Olivari (1996) suggest that it is rivulet location and not its profile or circumferential oscillation which initiates the response.

Several analytical models have also been developed to investigate RWIV, most of which are loosely based on the work of Yamaguchi (1990), wherein the RWIV mechanism is modelled as a two-dimensional, multiple mass, multiple degree of freedom (DOF), spring mass damper system, with aerodynamic forces determined using a quasi-steady approximation. These analytical models share several common features, but also present distinct differences determined by the exact nature of the specific aspect under investigation, two such examples being a 2DOF model with a circumferentially movable rigid attachment representing the 'artificial rivulet' (Gu and Huang, 2008), and a 4DOF three mass model to investigate the differences between laminar and turbulent flow on the cable-rivulet system response (Peil and Dreyer, 2007). Seidel and Dinkler (2006) investigated stable locations for the rivulets; however

in this instance the focus was on determining the differences between sub-critical and critical flow fields. The rivulets were considered as moveable disturbances, and the aerodynamic coefficients were determined using a theoretical approach based on Prandtl's tripwire phenomenon.

Despite all of this analytical work, however, computational models for RWIV are scarce due to the complexity of the problem and the need to couple models for the thin film of rain water, the unsteady aerodynamic field, and the structural dynamics of the cable. To date, the majority of the numerical investigations of RWIV have focused on fixed rigid artificial rivulets, with 2D and 3D large eddy simulations (LES) examining the effect that static rivulets have on the overall flow field (Li and Gu, 2006, Liu *et al*, 2007). Lemaitre *et al* (2007) presented a different approach using lubrication theory and the time averaged flow-field over a circular cylinder to ascertain the evolution of the rain water rivulets.

Research in the Departments of Mechanical Engineering and Mathematics at the University of Strathclyde has focused on developing a numerical model to investigate aspects of RWIV. The approach adopted is to couple a modified pre-existing unsteady aerodynamic solver for the external aerodynamic flow field with a solver based on a thin-film model for the evolution and deformation of the water rivulets. Results from the individual models will be presented herein along with preliminary results from fully coupled simulations of the problem.

INTERNATIONAL WORKSHOP ON RAIN-WIND INDUCED VIBRATION

An International Workshop on Rain-Wind Induced Vibration was hosted by the University of Strathclyde on 30th March to 1st April 2008. The Workshop was hosted by the authors of this paper at Ross Priory, a conference facility owned by the University of Strathclyde on the banks of Loch Lomond. The aim was to bring a number of the key international experts in the field of RWIV together to present and discuss their latest research findings on the phenomenon. The workshop format provided much more time for focussed and open discussion than is usually possible in a normal conference environment, allowing the current ideas and uncertainties on the underlying physics to be established and future research directions to be identified. Funding for the meeting was provided by the University of Strathclyde Research Enhancement Fund, and the delegates who attended the meeting were :

Dr Ian Taylor, Prof .Stephen Wilson, Dr Brian Duffy, Mr Andrew Robertson, Ms Julie Sullivan (University of Strathclyde),
Dr Xiaoqing Du (Tongji University, China),
Dr Olivier Flamand (CSTB Nantes, France),
Dr Pascal Hemon (LadHyX, Ecole Polytechnique, France),
Dr John Macdonald (University of Bristol, UK),

Prof. Masaru Matsumoto and Dr Tomomi Yagi (Kyoto University, Japan),
Dr Delong Zuo (Texas Tech University, USA),

and a photograph of the participants is shown in Fig. 2.

Summary of the Research Presented

During the Workshop, delegates presented recent and ongoing research on RWIV, in a more informal style than at conventional conferences. A brief summary of the content of these presentations is given below, followed by the main research themes that arose from the discussions.

The University of Strathclyde researchers highlighted the recent numerical developments in both the Department of Mechanical Engineering and Department of Mathematics, the results of which will be summarised later in this paper. In addition Prof. Stephen Wilson and Ms Julie Sullivan described some of the recent work in the Department of Mathematics on thin rivulets and ridges of fluid subject to prescribed longitudinal and/or transverse shear-stress effects at their free surface (Sullivan *et al*, 2008, Sullivan, 2009).

Prof. Matsumoto and Dr Yagi summarised the extensive research that has been conducted at Kyoto University. Particular themes included the role of the axial vortex on inclined cables (Matsumoto *et al*, 2001), the sensitivity of inclined cables to dry-state galloping (Matsumoto *et al*, 2007a), and the importance of Karman vortex suppression during the cable response associated with the negative lift slope when rivulets are present close to the separation points ((Matsumoto *et al*, 2001, Matsumoto *et al*, 2007a). Fig. 3 illustrates experimental results for artificial rivulets that exhibit the strong negative lift slope at about 50°.

Dr Flamand presented results from a series of wind tunnel tests which demonstrated that the surface characteristics of the cable play a strong role in the RWIV instability, notably for “dirty” cables (Flamand, 1995) and RWIV mitigation devices such as helical wires. Recent results (Cosentino *et al*, 2003) indicate that the water present on the cable forms a “base carpet” of constant height, on which an “oscillating wave” (the rivulet) slides. The frequency of this movement is the same as that of the cable motion, with the rivulet shape strongly influenced by inertia effects.

Dr Du gave a wide ranging summary of the research at Tongji University, China, under the leadership of Prof. Ming Gu. In particular, he presented high resolution pressure measurements illustrating the effect of artificial rivulets on the flow (Gu and Du, 2005, Gu and Huang, 2008, Gu, 2007), and results from theoretical models highlighting that when rivulets are present at certain circumferential locations the lift coefficient drops significantly and a galloping type instability is observed (Gu, 2007).

Dr Hemon presented recent experimental and numerical investigations focusing on the rivulet dynamics. Recent numerical computations have used lubrication theory to predict rivulet growth and evolution under a constant pressure loading, with two distinct rivulets being found to form at approximately the separation points of a dry circular cylinder under all the loadings examined (Lemaitre *et al*, 2007).

Dr Zuo provided details of numerous full scale investigations from the Fred Hartman Bridge, Houston, Texas, USA, reflecting on how re-analysis of existing data possibly changes the assessment of this instability (Zuo *et al*, 2008). Although comparisons of RWIV with vortex-induced vibration (VIV) illustrate similarities between the two phenomena, suggesting that RWIV may be due to a type of VIV excitation, the effect of the rivulets remains unclear.

Dr Macdonald summarised recent research on analytical modelling of dry-inclined galloping using a quasi-steady approach (Macdonald and Larose, 2008a, Macdonald and Larose, 2008b). A number of conjectures on the similarities between RWIV and dry-inclined galloping were considered, notably the effect of the critical Reynolds number and associated drag crisis on both instabilities.

Discussion : Key Research Themes and Future Research Directions

A main theme of the discussion was how RWIV can be categorised. The instability is distinct in many ways, thus meriting its own classification as a unique aeroelastic phenomenon. However, as outlined above, recent research has suggested that the phenomenon has characteristics related to a number of other instabilities which make it difficult to classify.

- Comparisons between full scale observations and dry-inclined galloping results indicate noticeable similarities between these two instabilities, particularly the effect of the critical Reynolds number regime.
- Rivulets located close to the separation points can suppress the Karman vortex, increasing the susceptibility of the cable to a galloping type instability.
- The presence of a low frequency axial vortex behind the inclined cable can cause a vortex-induced instability at high reduced velocity. The presence of rain water rivulets in certain locations on the cable surface can enhance this instability and the magnitude of the response (Matsumoto *et al*, 2001, Matsumoto *et al*, 2003).
- Similarities between classical VIV and RWIV have been identified, although RWIV occurs at higher reduced velocity and with higher amplitude than VIV.

The similarities between dry-inclined galloping and RWIV were a particular focus of the discussions. From experiments and full scale observations, it is

often problematic to classify or identify occurrences as either one type of instability or the other. Re-analysis of previous data has demonstrated that the two phenomena are not as distinct as previously thought. The general consensus was that the two phenomena are related, or are even potentially the same, and that the presence of rain water rivulets enhances or acts as a catalyst for the oscillation, perhaps “widening the window” for galloping. However, these ideas have not been conclusively demonstrated, and there are several unanswered questions as to the role of the rivulets on the overall flow field.

Considering the two instabilities as similar or related phenomena, however, may not be straightforward, as there have been instances of RWIV at fairly low speed and at sub-critical Reynolds numbers, which is not consistent with the general characteristics of dry-inclined galloping. Macdonald also confirmed that instances of “dry” vibrations at low wind speed have been reported, probably at sub-critical Reynolds numbers, where the oscillations are in a transverse or across-wind direction, which are not explainable by the quasi-steady theory. Recent numerical research from Yeo and Jones (2008) investigates the flow past a dry inclined cable at sub-critical Reynolds numbers. The results illustrate how swirling eddies are generated alternately from both sides of the cylinder but also move along the cylinder thus delaying the vortex shedding. This flow feature causes unsteady forces that vary both spatially and temporally in the spanwise direction, thus generating a low frequency loading on the cable. These results will provide a useful comparison for future investigations on the effect of rivulets on the 3D flow field around an inclined cable and their role in the generation or modification of the unsteady aerodynamic loading.

Reynolds number effects, particularly in the critical region, appear to be important to the mechanisms of both dry-inclined galloping and RWIV. Subsequently the “single-bubble” phenomenon † may play an important role, as identified by Cosentino *et al* (2003). This is a possible aspect of the RWIV mechanism that has not been fully investigated to date, with the role of the rivulets in enhancing or causing the single-bubble regime still not clear.

Rivulets located close to the separation point have a strong effect on the overall response, and rivulets at certain locations on the surface can cause large negative lift slopes, thus increasing the susceptibility to galloping (Matsumoto *et al*, 2007a, Matsumoto *et al*, 2008). Examples were given by both Flamand and Hemon of instances where a dry cable did not oscillate, but under the same flow conditions the introduction of water onto the surface of the cable

† The “single-bubble” region appears for flow close to the critical region, where one shear layer undergoes transition to a turbulent state, resulting in it separating later than the other shear layer, leading to asymmetric flow.

initiated oscillations. This indicates that the presence of the water is a key factor in the mechanism, although the role of the surface characteristics of the cable is not fully understood.

All of the delegates felt that the development of a numerical tool to investigate RWIV was important and could provide valuable data that has the potential to give important insights into the underlying physical mechanism of RWIV. However, the complexity of the problem has to date limited the development of a full numerical model. It was noted that any proposed model should incorporate numerical solutions of the Navier-Stokes equations for both the aerodynamic field and the water rivulets along with equations for the cable dynamics, and provide accurate unsteady pressure results.

The main conclusions from the International Workshop can therefore be summarised as follows :

- Despite considerable international research activity over the last two decades, the RWIV phenomenon is still not well understood.
- RWIV is related to, but distinct from, dry-inclined galloping.
- The presence of rivulets can act to increase the likelihood of a galloping-type oscillation.
- Vibrations often occur in flow regimes in which Karman vortex shedding is suppressed.
- RWIV often occurs in the critical Reynolds number range. However, the precise role of the drag crisis and the “single-bubble regime” has not yet been fully established.
- There is still a large degree of uncertainty as to the exact role played by the size, shape and location of the rivulets and the effect of surface characteristics.
- Improved numerical methods are required to aid understanding of RWIV, to provide information not presently obtainable from experiments and to help clarify several aspects of the phenomenon.

Furthermore, all of the delegates agreed that a similar workshop should be arranged in the future, in order to continue to stimulate ideas, communication and collaboration, and to further enhance understanding of RWIV.

NUMERICAL MODELLING OF RWIV

A numerical model for RWIV has been developed at the University of Strathclyde. The numerical approach used is to couple a thin-film model based on lubrication theory to an unsteady aerodynamic solver, the latter being a modified version of the DIVEX code developed at the Universities of Strathclyde and Glasgow, which has previously proven successful with unsteady, incompressible, highly separated flows such as those under investigation

(Taylor and Vezza, 1999, Taylor and Vezza, 2001, Taylor and Vezza, 2002). The thin-film model is based on an analytical model developed by the Department of Mathematics, which has a long track record of internationally recognised theoretical research into a wide variety of both steady and unsteady viscous thin-film flows, notably rivulet flows (Sullivan *et al*, 2008, Holland *et al*, 2001, Wilson and Duffy, 2005). The collaboration and complimentary skills of the two departments provides a unique team of researchers with the necessary capabilities to develop a numerical model for RWIV. A summary of some of the key results to date from this collaborative research are presented along with an indication of possible future research directions.

The Discrete Vortex Method

The governing equations used in the numerical model are the vorticity-stream function form of the continuity equation and the Navier-Stokes equations for two-dimensional incompressible viscous flow :

$$\nabla^2 \Psi = -\omega \ , \tag{1}$$

$$\frac{\partial \omega}{\partial t} + (\mathbf{U}.\nabla)\,\boldsymbol{\omega} = \nu \nabla^2 \boldsymbol{\omega} \ , \tag{2}$$

where the vorticity $\boldsymbol{\omega}$ is defined as the curl of the velocity (Eq. 3) and $\boldsymbol{\Psi}$ is a vector potential (Eq. 4).

$$\boldsymbol{\omega} = \nabla \times \mathbf{U} \quad \text{with} \quad \boldsymbol{\omega} = \omega\,\mathbf{k} \ , \tag{3}$$

$$\mathbf{U} = \nabla \times \boldsymbol{\Psi} \ , \quad \nabla.\boldsymbol{\Psi} = 0 \quad \text{with} \quad \boldsymbol{\Psi} = \Psi\,\mathbf{k} \ . \tag{4}$$

The far field boundary conditions (Eq. 5), and no-slip and no-penetration conditions (Eq. 6) apply at infinity and the surface of the body, respectively,

$$\mathbf{U} = \mathbf{U}_\infty \quad \text{or} \quad \nabla\Psi = \nabla\Psi_\infty \quad \text{on} \quad S_\infty \ , \tag{5}$$

$$\mathbf{U} = \mathbf{U}_i \quad \text{or} \quad \nabla\Psi = \nabla\Psi_i \quad \text{on} \quad S_i \ , \tag{6}$$

where subscripts ∞ and *i* respectively denote the far field and the *i*th body (*i* = 1, 2, .. *m*, with *m* being the number of solid bodies). Proper definition of the problem allows only one of the normal and tangential boundary conditions at the body surface to be explicitly applied. In the current formulation, this is the normal component no-penetration condition. However, the tangential no-slip condition is implicitly satisfied due to the representation of the internal kinematics of each solid body. The velocity at a point $\mathbf{r}$ on the surface of or within body *i* can be described by

$$\mathbf{U}_i = \mathbf{U}_{ic} + \Omega_i \times (\mathbf{r}_p - \mathbf{r}_{ic}) \ , \tag{7}$$

where $\mathbf{r}_{ic}$ is a fixed reference point on the body. This may be represented in stream-function form as

$$\nabla^2 \Psi_i = -2\Omega_i \quad \text{in} \quad B_i \ . \tag{8}$$

Application of Green's theorem to Eq. (1) and (8), together with boundary conditions Eq. (5) and (6), allows a relationship between velocity and vorticity to be obtained. The velocity field can then be calculated using the Biot-Savart law, which expresses it in terms of the vorticity field. For a point *p* in the fluid, the velocity is given by

$$\mathbf{U}_p = \mathbf{U}_\infty + \frac{1}{2\pi}\int_F \omega \frac{\mathbf{k}\times(\mathbf{r}_p - \mathbf{r})}{\left\| \mathbf{r}_p - \mathbf{r} \right\|^2} dF + \int_{B_i} 2\Omega_i \frac{\mathbf{k}\times(\mathbf{r}_p - \mathbf{r})}{\left\| \mathbf{r}_p - \mathbf{r} \right\|^2} dB_i \quad . \tag{9}$$

The pressure distribution on the body surface can then be evaluated by integrating the pressure gradient along the body contour, which is given by

$$\frac{1}{\rho}\frac{\partial P}{\partial s} = -\mathbf{s}.\frac{D\mathbf{U}_c}{D\,t} - \mathbf{n}.(\mathbf{r}-\mathbf{r}_c)\frac{D\Omega}{D\,t} + \mathbf{s}.(\mathbf{r}-\mathbf{r}_c)\,\Omega^2 + \nu\frac{\partial\omega}{\partial\, n} \quad . \tag{10}$$

The resulting pressure distribution can then be integrated around the body surface to calculate the aerodynamic forces on the body and the moment about the body reference point, $\boldsymbol{r}_{ic}$, at a particular computational time step. Further statistical measures such as time-averaged mean coefficients may then be determined. For a more detailed presentation of the details as they relate to the present numerical implementation the reader is referred to Taylor and Vezza (1999).

Mathematical Modelling of the Rivulet Dynamics

Two-dimensional, unsteady flow of a thin film of incompressible viscous fluid with uniform dynamic viscosity μ and density ρ on the outer surface of a stationary horizontal circular cylinder of radius *R* is considered. The free surface of this film is subject to a prescribed normal stress ('pressure'), $P = P(\theta, t)$, and prescribed tangential stress ('shear'), $T = T(\theta, t)$, exerted by the external aerodynamic field (Fig. 4). The evolution equation for the water thickness on the cylinder surface, $h(\theta, t)$, is given by

$$h_t + \left[-\frac{1}{3\mu R}\left(\rho g \cos\theta - \frac{\gamma}{R^3}(h + h_{\theta\theta})_\theta + \frac{P_\theta}{R} \right) h^3 + \frac{Th^2}{2\mu R} \right]_\theta = 0 \quad , \tag{11}$$

the full derivation of which is given in Appendix A. Eq. (11) is consistent with the corresponding equation given by Lemaitre et al (2007) in the case of flow on a static cylinder. This equation is to be solved subject to an initial condition of the form $h(\theta, 0) = h_0(\theta)$, where $h_0(\theta)$ is the initial thickness of the film. For definiteness in the present work we have chosen an initially uniform film $h_0 =$ *constant*, and allow the film to evolve according to Eq. (11) to see if two-dimensional 'rivulets' develop.

RESULTS OF THE NUMERICAL INVESTIGATION

Investigation of Artificial Rivulets

A numerical investigation to ascertain the effect of the circumferential location of artificial rivulets on the overall flow field was undertaken. As Robertson and Taylor (2007) describe in more detail, the artificial rivulet used is a trapezoidal profile and is a similar size and shape to those used in recent wind tunnel studies (Fig. 5a). In all cases, a sub-critical Reynolds number, *Re* = 2×10^4 (based on the cable diameter), was used and is consistent with the lower wind speed range for RWIV.

Two combinations of rivulet geometry, referred to as single and multiple symmetric rivulet (Fig. 5b), are presented herein. A multiple antisymmetric configuration is also presented by Robertson and Taylor (2007). These particular arrangements were chosen to best represent possible rivulet configurations governed by a single angular parameter, θ.

a) Single Rivulet

The upper rivulet is thought to play the greatest role in RWIV. As such, the primary study examined the variation of aerodynamic force coefficients on the cylinder with angle of the attached rivulet from incident flow, θ. The variation of predicted time-averaged mean aerodynamic forces with rivulet location is shown in Fig. 6, where the lift shows good agreement with results from experimental data (Matsumoto *et al*, 2007b).

The presence of the rivulet on the cable surface leads to four distinct flow regimes which can be clearly identified in the aerodynamic force results. At angles θ < 45° the attached rivulet has little effect on either of the mean aerodynamic coefficients (lift $\overline{C_L}$ and drag $\overline{C_D}$) in comparison to the dry cylinder case, as the rivulet is located too close to the front of the cylinder for it to have a significant effect on the separation of the shear layers and wake formation. The rivulet does cause a local separation of the shear layer, though at these low angles the flow almost immediately reattaches to the cylinder, with full separation occurring only at the same location as a dry cylinder. Hence the overall mean loadings are not strongly affected, as is also demonstrated by the experimental results, where the lift is determined to be zero until approximately 35°. The experiments (Matsumoto *et al*, 2007b) used a slightly higher Reynolds number of 2.6×10^4, which may give some explanation for the increase in lift occurring at a slightly lower angle due to the effect of *Re* on the boundary-layer formation.

At $\theta \cong 45°$ a sudden change in flow regime occurs, with a rapid increase in time-averaged mean lift coefficient and a corresponding but much smaller

decrease in time-averaged mean drag coefficient. This occurs because the rivulet is now sufficiently far from the stagnation point that it causes the boundary layer to trip, thus influencing the location of the separation point on the upper side of the cylinder. This transition to turbulent flow on the upper side causes the flow to detach at a greater angle from incidence than the laminar flow on the lower (non-rivulet) side, which results in an asymmetric flow field generating a positive lift force, towards the side of the rivulet.

At angles above $\theta \cong 60°$ the tripped flow on the upper surface detaches from the cylinder at the rivulet location, and this probably occurs earlier than on the lower surface. The resulting asymmetric flow with negative lift (towards the opposite side from the rivulet) and the increase in cross-flow wake size are caused by the detachment of the flow, which also results in an increase in the drag.

When the angle is greater than $\theta \cong 100°$, the rivulet is located sufficiently far past the separation point to ensure that it is in the region of the cylinder surface that is immersed in the wake and thus has a negligible impact on the aerodynamic properties of the body itself.

Crucially in the second of these regimes, $50° < \theta < 60°$, unlike at any other angular position, Karman vortex shedding is suppressed and no clear Strouhal frequency can be detected. The negative lift curve slope in this region suggests that this could lead to a potential galloping instability, and at these angles the Den Hartog criterion, $\frac{dC_L}{d\theta} + C_D < 0$, was found to be valid.

b) Multiple Symmetric Rivulets

In this case the rivulets are located symmetrically at equal angles clockwise and anti-clockwise from the incident flow. The predicted variation of $\overline{C_L}$ with θ is shown in Fig. 7. These results demonstrate features that are consistent with phenomena discussed in the single rivulet case. Notably the symmetry of the problem gives zero mean lift over almost the entire range of rivulet angle, and hence in this case no galloping instability could occur. (Symmetry means that $\frac{dC_L}{d\theta} \approx 0$ at all angles, so the Den Hartog criterion is not satisfied.) The exception occurs when $\theta \cong 50°$, where experiments (Matsumoto *et al*, 2008) have shown that the flow field is very sensitive to small changes in the rivulet position. This sensitivity is still being investigated in the present numerical study and will be fully reported in future. Distinct similarities to the single rivulet case are also apparent in the $\overline{C_D}$ profile, one example being the increase in mean drag coefficient in the range $60° < \theta < 100°$ due to the detachment of the flow, resulting in a wider wake.

c) Oscillating Rivulet

Simulations were undertaken with the rivulet oscillating sinusoidally with constant amplitude on the surface of the cylinder. Due to the greater complexity of the flow field and larger number of variables, interpreting the results becomes increasingly difficult. Of particular interest are cases when the rivulet oscillates in the region where the changes in lift and drag were greatest in the static artificial rivulet analysis presented above. Furthermore, unless the rivulet is located within the wake, $\theta \geq 100°$, markedly increased local "jumps" in the pressure field can be seen as the flow is tripped by the rivulet before separation, as shown in Fig. 8. The location of the flow re-attachment on the cylinder surface and the subsequent effects that this has on the time-averaged aerodynamic forces depends on the frequency and amplitude of the oscillation. Full analysis of the oscillating rivulets case is ongoing and will be reported in the future.

Numerical Analysis of the Thin Film of Water

The evolution equation (Eq. 11) is a fourth order, non-linear, non-constant coefficient partial differential equation, and as such it cannot, in general, be solved analytically. Therefore, a pseudo-spectral (or collocation) method solver using an *N* point Fourier spectral mode in space and a fourth-order Adams-Bashforth time-marching algorithm was constructed. This numerical method was chosen specifically because of the periodic and continuous nature of the problem over the interval $\theta \in [0°, 360°)$, and the rapid rate of convergence it provides to the solution, given the presumed smoothness of the final result. Further details of the implementation of the pseudo-spectral method and parameter selection are given in Robertson et al (2008).

Standard values for gravity and the properties at an air-water interface at 20°C were used throughout the present study and are listed in Table 2, while other parameter values were chosen to represent typical values for RWIV and to ensure the ratio of initial film thickness to cylinder radius $h_0/R = 6.3 \times 10^{-3}$ was consistent with those of previous experimental and computational studies by Flamand (1995) and Lemaitre *et al* (2007). Accordingly, the Reynolds number implemented was a sub-critical value typical for RWIV of $Re = 10^5$.

The distributions of pressure and shear due to the external aerodynamic field were assumed to be constant with time and therefore functions of θ only, i.e. $P = P(\theta)$ and $T = T(\theta)$, illustrated in Fig. 9. These are based upon the mean pressure coefficient and normalised mean friction coefficients, $\overline{C}_P$ and $\overline{C}_F{}^*$, for the external aerodynamic field around a dry cylinder, values for which were determined experimentally by Achenbach (1968) at a Reynolds number similar to that under investigation here of $Re = 10^5$. For the numerical investigation,

twenty-term Fourier series representations of $\overline{C}_P$ and $\overline{C}_F{}^*$ were used and appropriately scaled such that the maximum values of pressure and shear loadings matched those of Lemaitre *et al* (2007), thus allowing direct comparisons between the results.

Three different combinations of the loadings, pressure *P*, shear *T*, surface tension γ and gravity *g* were considered in this study. These were

(a) shear and surface tension (*P* ≡ 0 and *g* = 0),

(b) pressure and surface tension (*T* ≡ 0 and *g* = 0),

(c) full loading (*P, T, g* and $\gamma \neq 0$).

a) Shear and Surface Tension Loading

The temporal evolution of the thin film under the effect of shear *T* and surface tension γ loading is shown in Fig. 10. Under this combination, two distinct symmetrically placed rivulets form, one each on the upper and lower surfaces, with locations just windward of the clockwise and anti-clockwise separation points for a dry cylinder at the same *Re*. As expected for this shear loading, the two rivulets are of equal height, profile and growth rate. This prediction is consistent with the previous experimental analysis of Bosdogianni and Olivari (1996), who indicate that the rivulets "form on the upper and lower surface of the cylinder at positions roughly corresponding to the expected separation points". The results are also in good agreement with the only other computational results available for the same problem (Lemaitre *et al*, 2007) illustrated in Fig. 11, which demonstrates that the present results are virtually the same as those obtained by Lemaitre *et al* (2007), at an evolution time of *t* = 6.9×10^{-3} s. Although both sets of results are numerical predictions, the governing evolution equations (eq. (11) from above, and eq. (17) from Lemaitre *et al*, 2007) were independently derived and were solved via different procedures, thus verifying the computational results.

b) Pressure and Surface Tension Loading

Under only pressure *P* and surface tension γ loading, the results show distinct similarities to those for the previous case. Here again symmetric rivulets form just windward of the separation points on both sides of a dry cylinder (Figs. 12 and 13). In this instance, however, the locations of these rivulets are marginally windward of those formed in the shear and surface tension case (Fig. 13), with the 'size' of the rivulets under the present pressure loading being approximately the same order of magnitude as for the shear loading condition. When considered in conjunction with the similar rates of rivulet growth (Figs. 10 and 12), the indication is that the effects of pressure and shear loadings are of a similar magnitude and therefore appear to be of broadly equal importance.

c) Full Loading

The temporal evolution of film thickness for all four loading conditions (pressure, shear, surface tension and gravity) acting simultaneously is shown in Fig. 14. Similarly to the previous two cases, under full loading conditions two distinct rivulets can be seen to form. However, in this instance the symmetry with respect to the incident flow between the upper and lower surfaces of the cylinder is lost due to the effect of gravity. The gravitational loading causes the rivulets to be thicker on the lower surface and thinner on the upper surface than those examined previously. The growth rate of the lower rivulet is also greater than that of the upper rivulet due to the effect of gravitational loading, as would be expected. Furthermore, while the point of maximum thickness of the lower rivulet moves leeward from the point where it occurred under pressure and surface tension loading only, specifically from $\theta \approx 288°$ to $\theta \approx 282°$, the thinner upper rivulet moves windward from $\theta \approx 66°$ to $\theta \approx 59°$.

Fully Coupled Model

Research is ongoing to develop a fully coupled model using the rivulet evolution equation and the unsteady aerodynamic solver. The coupled model uses the pressure predicted by the unsteady solver as input to the rivulet evolution equation to determine the film thickness (gravity not included). The new surface distribution of the film is then used as input to the next timestep of the aerodynamic solver, to determine the new external flow field and pressure, and the process is repeated. Images at various stages of the rivulet growth from initial simulations are illustrated in Fig. 15. These preliminary results from this unique coupled model demonstrate the capability of this model to provide a numerical tool capable of simulating RWIV. The nature of the rivulets predicted by the unsteady coupled simulation are noticeably different from the results presented above that used a constant pressure distribution. This is as expected since in the above case, the pressure and shear distributions are unaffected by the formation of the rivulets, whereas in the coupled model the rivulet profile and shape, as well as the pressure and shear distributions, are changing in time. Most noticeably, two “bulges” are formed on the upper and lower surfaces of the cylinder. The initial interpretation is that the upstream rivulet forms close to the separation point, and the downstream rivulet evolves due to the reattachment of the shear layer. As the thickness of the upstream rivulet increases, the separation and reattachment of the shear layer is affected and the downstream rivulet moves forward. It does appear that for the wind speed used in this investigation, the rivulets move towards an “equilibrium” angle (close to the separation point for a dry cylinder), after which there is no apparent further motion, although the shapes of the rivulets are still changing with time.

These results show that the method has the potential to allow a detailed investigation into the rivulet dynamics and their effect on the unsteady loading on the cylinder. However, the results and interpretations are preliminary and research is ongoing to develop the numerical model further.

CONCLUSIONS

Rain-wind induced vibration is an active area of research, with the underlying physical mechanisms of the phenomenon still to be fully understood. At a recent International Workshop on RWIV, the following key themes and areas for future research activity were identified :

- RWIV is still not well understood.
- RWIV is related to, but distinct from, dry-inclined galloping.
- The presence of rivulets can act to increase the likelihood of a galloping-type oscillation.
- Vibrations often occur in flow regimes in which Karman vortex shedding is suppressed.
- RWIV often occurs in the critical Reynolds number range, though the full effect of the Reynolds number variation has not been fully established.
- The effect of the size, shape and location of the rivulet and the effect of surface characteristics has not been fully determined.
- Improved numerical methods are required to aid understanding of RWIV.

A numerical method to investigate aspects of RWIV has been developed at the University of Strathclyde, which uses an unsteady aerodynamic solver for the external aerodynamic field and a thin-film model based on lubrication theory to model the rivulet evolution and motion. Results from the new modelling approach are presented, and the main conclusions are :

- Artificial rivulets on the cylinder modify the aerodynamic force coefficients (which vary with rivulet angle), and at particular rivulet configurations can cause a susceptibility to a galloping type instability.
- Results obtained from the thin-film model are consistent with those in the literature. Under shear or pressure loading two symmetric rivulets form just windward of the separation points, while under full loading conditions the rivulets are asymmetric due to the additional effect of gravity.
- Preliminary results from a fully coupled model demonstrate how the changing flow field influences the rivulet motion and growth.

ACKNOWLEDGEMENTS

The authors would like to thank the University of Strathclyde Research Enhancement Fund for providing the funds for the International Workshop. We

would also like to thank all the delegates who attended the Workshop for entering into a full and open discussion. Without the willingness of these delegates to kindly offer their time and expertise, the workshop would not have been a success : Dr Xiaoqing Du, Dr Olivier Flamand, Dr Pascal Hemon, Dr John Macdonald, Prof. Masaru Matsumoto, Dr Tomomi Yagi and Dr Delong Zuo.

Thanks also to Mrs Irene Spencer, Department of Mathematics, University of Strathclyde, for undertaking many of the organisational arrangements for the Workshop.

The authors A.C. Robertson and J.M. Sullivan gratefully acknowledge the support of the UK Engineering and Physical Sciences Research Council (EPSRC) via Doctoral Training Account studentships.

REFERENCES {TO DO FROM HERE}

Achenbach, E. (1968). Distribution of local pressure and skin friction around a circular cylinder in a cross flow up to *Re* = 5 × 10^6. *Journal of Fluid Mechanics*, **34**, 625-639.

Bosdogianni, A. & Olivari, D. (1996). Wind- and rain-induced oscillations of cables of stayed bridges. *Journal of Wind Engineering and Industrial Aerodynamics*, **64**, No. 2-3, 171-185.

Cosentino, N., Flamand, O. & Ceccoli, C. (2003). Rain-wind induced vibration of inclined stay cables. Part 1: experimental investigation and physical explanation. *Wind and Structures*, **6**, No. 6, 471–484.

Flamand, O. (1995). Rain-wind induced vibration of cables. *Journal of Wind Engineering and Industrial Aerodynamics*, **57**, 353–362.

Geurts, C., Vrouwenvelder, T., Van Staalduinen, P. & Reusink, J. (1998). Numerical modelling of rain-wind-induced vibration : Erasmus Bridge, Rotterdam. *Structural Engineering International, Journal of the International Association for Bridge and Structural Engineering*, **8**, No. 2, 129-135.

Gu, M., Liu, C.J., Xu, Y.L., & Xiang, H.F. (2002). Response characteristics of wind excited cables with artificial rivulet. *Applied Mathematics and Mechanics*, **23**, 1176–1187.

Gu, M. & Du, X. (2005). Experimental investigation of rain-wind-induced vibration of cables in cable-stayed bridges and its mitigation. *Journal of Wind Engineering and Industrial Aerodynamics*, **93**, 79-95.

Gu, M. (2007). Study on wind-rain induced vibration of stay cables of cable-stayed bridges based on quasi-steady assumption. *Proceedings of the 12th International Conference on Wind Engineering, Cairns, Australia*, *July 2007*, 895-902.

Gu, M. & Huang, L. (2008). Theoretical and experimental studies on the aerodynamic instability of a two-dimensional circular cylinder with a moving attachment. *Journal of Fluids and Structures*, **24**, 200-211.
Hikami, Y. & Shiraishi, N. (1988). Rain-Wind induced vibrations of cables in cable stayed bridges. *Journal of Wind Engineering and Industrial Aerodynamics*, **29**, No. 1-3, 409-418.
Holland, D., Duffy, B.R. & Wilson, S.K. (2001). Thermocapillary effects on a thin viscous rivulet draining steadily down a uniformly heated or cooled slowly varying substrate. *Journal of Fluid Mechanics*, **441**, 195-221.
Lemaitre, C., Hemon, P. & De Langre, E. (2007) Thin water film around a cable subject to wind. *Journal of Wind Engineering and Industrial Aerodynamics*, **95**, 1259-1271.
Li, S.Y. & Gu, M. (2006). Numerical simulations of flow around stay cables with and without fixed artificial rivulets. *Proceedings of the 4th International Symposium on Computational Wind Engineering (CWE2006), Yokohama, Japan, July 2006*, 307-310.
Liu, Q., Matsumoto, M., Yagi, T. & Hori, K. (2007) LES study on the mechanism of rain-wind induced vibration of cables of cable-stayed bridge. *Proceedings of the 12th International Conference on Wind Engineering, Cairns, Australia, July 2007*, 895-902.
Macdonald, J.H.G. & Larose, G.L. (2008a). Two-degree-of-freedom inclined cable galloping. Part 1: General formulation and solution for perfectly tuned system. *Journal of Wind Engineering and Industrial Aerodynamics*, **96**, 291-307.
Macdonald, J.H.G. & Larose, G.L. (2008b). Two-degree-of-freedom inclined cable galloping. Part 2: Analysis and prevention for arbitrary frequency ratio. *Journal of Wind Engineering and Industrial Aerodynamics*, **96**, 308-326.
Matsumoto, M., Saitoh, T., Kitazawa, M., Shirato, H., & Nishizaki, T. (1995). Response characteristics of rain-wind induced vibration of stay-cables of cable-stayed bridges. *Journal of Wind Engineering and Industrial Aerodynamics*, **57**, 323-333.
Matsumoto, M., Yagi, T., Shigemura, Y. & Tsushima, D. (2001). Vortex-induced cable vibration of cable-stayed bridges at high reduced velocity. *Journal of Wind Engineering and Industrial Aerodynamics*, **89**, 633-647.
Matsumoto, M., Yagi, T., Goto, M. & Sakai, S. (2003). Rain-wind induced vibration of inclined cables at limited high reduced wind velocity region. *Journal of Wind Engineering and Industrial Aerodynamics*, **91**, 1–12.
Matsumoto, M., Yagi, T., Hatsuda, H., Shima, T. & Tanaka, M. (2007a). Sensitivity of dry-state galloping of cable stayed bridges to Scruton number.

Proceedings of 7th International Conference on Cable Dynamics, Vienna, Austria, *December 2007*, Paper no. 6.
Matsumoto, M., Yagi, T., Adachi, Y., Hatsuda, H. & Shima, T. (2007b) Karman vortex effects on aerodynamic instabilities of inclined stay-cables. *Proceedings of the 12th International Conference on Wind Engineering, Cairns, Australia*, *July 2007*, 175-182.
Matsumoto, M., Hashimoto, M., Yagi, T., Nakase, T. & Maeta, K. (2008). Study on the role of Karman Vortex on galloping of bluff bodies. *Proceedings of the 9th International Conference on Flow-Induced Vibration – FIV2008, Prague, Czech Republic, July 2008*, 687-692.
Ni, Y.Q., Wang, X.Y., Chen, Z.Q. & Ko, J.M. (2007). Field observations of rain-wind-induced cable vibration in cable-stayed Dongting Lake Bridge. *Journal of Wind Engineering and Industrial Aerodynamics*, **95**, No. 5, 303-328.
Peil, U. & Dreyer, O. (2007). Rain-wind induced vibrations of cables in laminar and turbulent flow. *Wind and Structures*, **10**, 83-97.
Robertson, A.C. & Taylor, I.J. (2007). Effect of rivulets on a circular cylinder using a 2D discrete vortex method. *Proceedings of the 12th International Conference on Wind Engineering, Cairns, Australia*, *July 2007*, 863-870.
Robertson, A.C., Taylor, I.J., Wilson, S.K., Duffy, B.R. & Sullivan, J.M. (2008). A model for the numerical simulation of rivulet evolution on a circular cylinder in an air flow. *Proceedings of the 9th International Conference on Flow-Induced Vibration – FIV2008, Prague, Czech Republic, July 2008*, 693-698.
Seidel, C. & Dinkler, D. (2006). Rain-wind induced vibrations – phenomenology, mechanical modelling and numerical analysis. *Computers and Structures*, **84**, No. 24-25, 1584-1595.
Sullivan, J.M., Wilson, S.K. & Duffy, B.R. (2008). A thin rivulet of perfectly wetting fluid subject to a longitudinal surface shear stress. *Quarterly Journal of Mechanics and Applied Mathematics*, **61**, No. 1, 25-61.
Sullivan, J.M. (2009). Thin-film flows subject to an external shear stress. *Ph D Thesis, Department of Mathematics, University of Strathclyde, Glasgow, UK*.
Taylor, I.J. & Vezza, M. (1999). Prediction of unsteady flow around square and rectangular section cylinders using a discrete vortex method. *Journal of Wind Engineering and Industrial Aerodynamics*, **82**, No. 1–3, 247–269.
Taylor, I.J. & Vezza, M. (2001). Application of a discrete vortex method for the analysis of suspension bridge deck section. *Wind and Structures*, **4**, No. 4, 333–352.
Taylor, I.J. and Vezza, M. (2002). Aeroelastic stability analysis of a bridge deck with added vanes using a discrete vortex method. *Wind and Structures*, **5**, No. 2–4, 277–290.

Verwiebe, C. & Ruscheweyh, H. (1998). Recent research results concerning the exciting mechanisms of rain-wind-induced vibrations. *Journal of Wind Engineering and Industrial Aerodynamics*, **74-76**, 1005-1013.
Wang, Z.J., Zhou, Y., Huang, J.F & Xu, Y.L. (2005). Fluid dynamics around an inclined cylinder with running water rivulets. *Journal of Fluids and Structures*, **21**, 49-64.
Wilson, S.K. & Duffy, B.R. (2005). Unidirectional flow of a thin rivulet on a vertical substrate subject to a prescribed uniform shear stress at its free surface. *Physic of Fluids*, **17**, No. 10, 108105.
Yamaguchi, H. (1990). Analytical study on the growth mechanism of rain vibration of cables. *Journal of Wind Engineering and Industrial Aerodynamics*, **33**, 78-80.
Yeo, D. & Jones, N.P. (2008). Investigation on 3-D characteristics of flow around a yawed and inclined circular cylinder. *Journal of Wind Engineering and Industrial Aerodynamics*, **96**, No. 10-11, 1947-1960.
Zuo, D., Jones, N.P. & Main, J.A. (2008). Field observation of vortex- and rain-wind-induced stay-cable vibrations in a three-dimensional environment. *Journal of Wind Engineering and Industrial Aerodynamics*, **96**, No. 6-7, 1124-1133.

APPENDIX A :

DERIVATION OF THIN FILM EQUATIONS.

Two-dimensional, unsteady flow of a thin film of incompressible viscous fluid with uniform dynamic viscosity μ and density ρ on the outer surface of a stationary horizontal circular cylinder of radius R is considered. The free surface of this film is subject to a prescribed normal stress ('pressure'), $P = P(\theta, t)$, and prescribed tangential stress ('shear'), $T = T(\theta, t)$, exerted by the external aerodynamic field (Fig. 4), as a function of clockwise angle from the windward (left-hand) horizontal, θ ($0° \le \theta \le 360°$), and time, t.

Model Description

We take the film to be thin, its aspect ratio ε (defined by $\varepsilon = H/R$, where H denotes a typical film thickness) satisfying $\varepsilon << 1$ (Fig. 4).

Initially we refer the description to polar coordinates r, θ, z with the z axis along the axis of the cylinder and with θ ($-\pi < \theta \le \pi$) measured from the horizontal on the upstream (left-hand) side of the cylinder; then the surface of the cylinder is given by $r = R$. We denote film thickness by $h = h(\theta, t)$ (unknown *a priori*); then the free surface of the film is given by $r = R + h$. Near any station $\theta = constant$ we may alternatively refer the description to a local Cartesian coordinate system $Oxyz$ with Ox tangential to the cylinder (increasing in the

direction of increasing θ, so that $x = R\theta$ + *constant*) and *Oy* along the outward normal to the cylinder, with y defined by $y = r - R$, so that the cylinder is at $y = 0$ and the free surface is at $y = h$. In the latter coordinate system the governing mass-conservation and Navier–Stokes equations give, at leading order in ε,

$$u_x + v_y = 0 \ , \tag{A.1}$$

$$0 = -p_x - \rho g \cos\theta + \mu u_{yy} \ , \tag{A.2}$$

$$0 = -p_y \ , \tag{A.3}$$

where we have written

$$\mathbf{u}(r,\theta) = \mathbf{i}u(r,\theta) + \mathbf{j}v(r,\theta) \qquad \text{and} \qquad \mathbf{g} = -g\left(\mathbf{i}\cos\theta + \mathbf{j}\sin\theta\right). \tag{A.4}$$

Equations (A.1)–(A.3) are subject to the no-slip and no-penetration conditions on the cylinder:

$$u = v = 0 \quad \text{on} \quad y = 0 \, , \tag{A.5}$$

and at the free surface, to the kinematic condition

$$v = h_t + uh_x \quad \text{on} \quad y = h \ , \tag{A.6}$$

the tangential stress condition

$$\mu u_y = T \quad \text{on} \quad y = h \ , \tag{A.7}$$

and the normal stress condition

$$p = \gamma\kappa + P \quad \text{on} \quad y = h \ , \tag{A.8}$$

where γ is the coefficient of surface tension, and κ is the mean curvature of the free surface, given to first order by

$$\kappa = \frac{1}{R} - \frac{1}{R^2}\left(h + h_{\theta\theta}\right) \ . \tag{A.9}$$

The azimuthal volume flux of fluid in the film is given by

$$Q = \int_0^h u \, dy \ , \tag{A.10}$$

and using this and (A.1) we may replace (A.6) by the conservation law

$$h_t + Q_x = 0 \ . \tag{A.11}$$

Evolution Equation for *h*(θ, *t*)

Integrating (A.3) subject to (A.8) we obtain

$$p = \gamma\kappa + P \tag{A.12}$$

(independent of *y*), and then integrating (A.2) with respect to *y* subject to (A.5) and (A.7) we obtain

$$u = -\frac{1}{2\mu}\left(\rho g\cos\theta + p_x\right)\left(2hy - y^2\right) + \frac{Ty}{\mu} \ . \tag{A.13}$$

Therefore from (A.10)

$$Q = -\frac{1}{3\mu}\left(\rho g\cos\theta + p_x\right)h^3 + \frac{Th^2}{2\mu} \ . \tag{A.14}$$

Finally, substituting (A.14) into (A.11) and using (A.9) and (A.12) leads to the evolution equation for $h(\theta, t)$:

$$h_t + \left[-\frac{1}{3\mu R}\left(\rho g \cos\theta - \frac{\gamma}{R^3}\left(h + h_{\theta\theta}\right)_\theta + \frac{P_\theta}{R} \right) h^3 + \frac{Th^2}{2\mu R} \right]_\theta = 0 . \qquad \text{(A.15)}$$

Figures

Figure 1. Definition of cable orientation, defining the angle of inclination α, and yaw angle β.

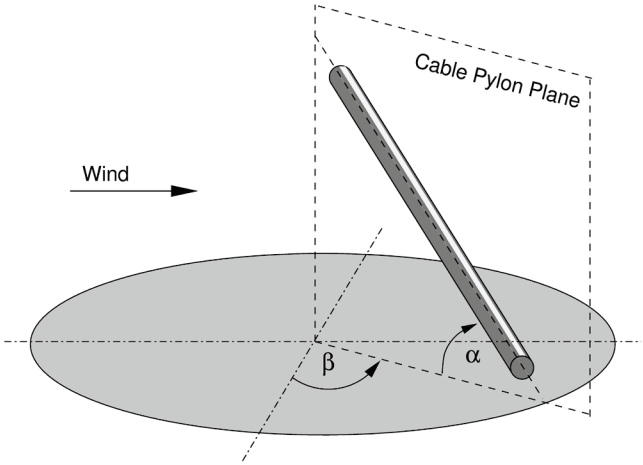

Figure 2. The participants in the International Workshop on Rain-Wind Engineering, held at Ross Priory, University of Strathclyde, 30th March – 1st April 2008. From left to right : Prof. Stephen Wilson, Dr Brian Duffy, Dr Xiaoqing Du, Dr John Macdonald, Dr Olivier Flamand, Prof. Masaru Matsumoto, Dr Pascal Hemon, Dr Delong Zuo, Dr Ian Taylor, Ms Julie Sullivan, Dr Tomomi Yagi, Mr Andrew Robertson.

Figure 3. Steady lift slope $dC_L/d\theta$ as a function of θ for a circular cylinder with symmetrical artificial rivulets (reproduced with kind permission from Prof. Matsumoto and taken from Matsumoto *et al*, 2008).

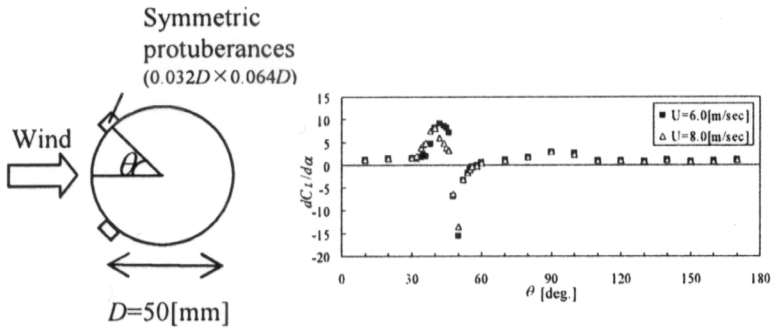

Figure 4. A thin fluid film on a horizontal cylinder.

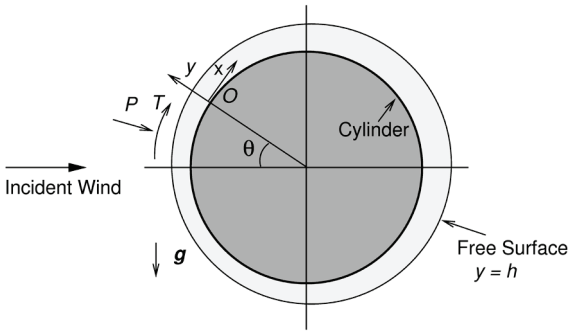

Figure 5. Modelling of artificial rivulets :

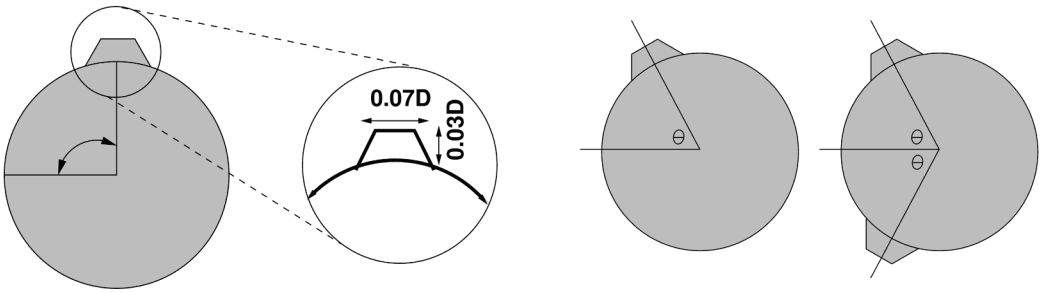

a) Profile and dimensions of the artificial rivulet (rivulet size enlarged for purposes of clarity).

b) Two-rivulet models: single and multiple symmetric.

Figure 6. Variation of $\overline{C_D}$ and $\overline{C_L}$ with rivulet angle θ for the single artificial rivulet case, compared with experimental data from Matsumoto *et al* (2007b).

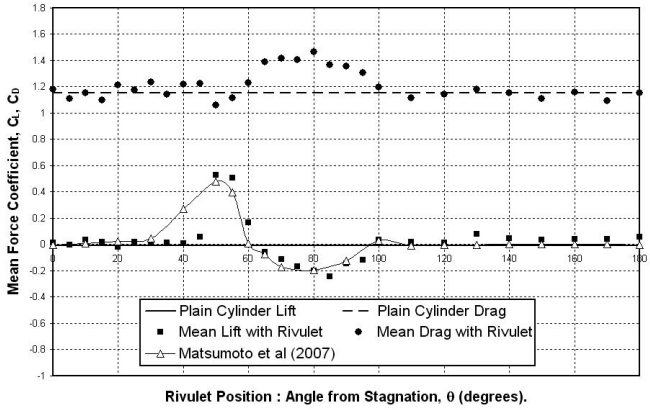

Figure 7. Variation of $\overline{C_D}$ and $\overline{C_L}$ with rivulet angle θ for the multiple symmetric artificial rivulet case.

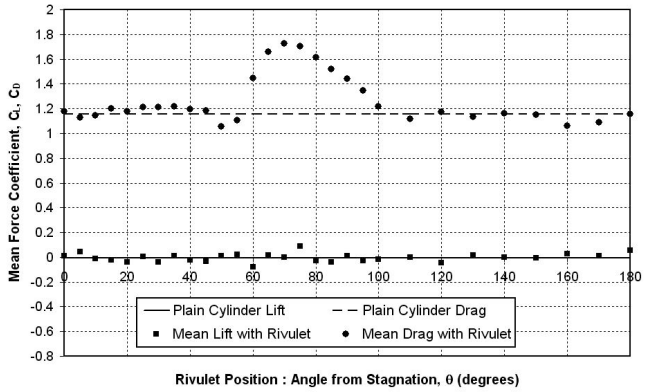

Figure 8. Instantaneous pressure coefficient for symmetrically oscillating rivulets (flow from left) :

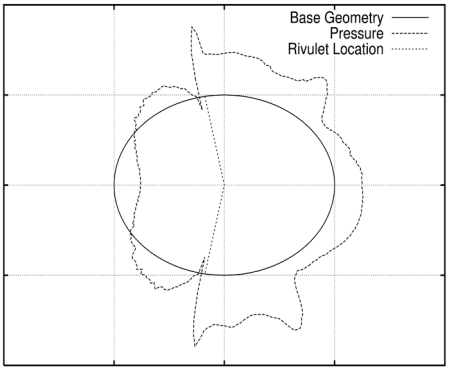

(a) Pressure "jump" when rivulet not located in wake.

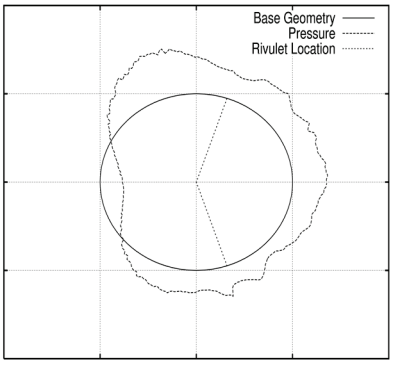

(b) No pressure "jump" when rivulet located in wake.

Figure 9. Aerodynamic coefficients $\overline{C}_P$ and $\overline{C}_F{}^*$ used in the numerical calculations and those measured experimentally by Achenbach (1968) for *Re* = 10^5.

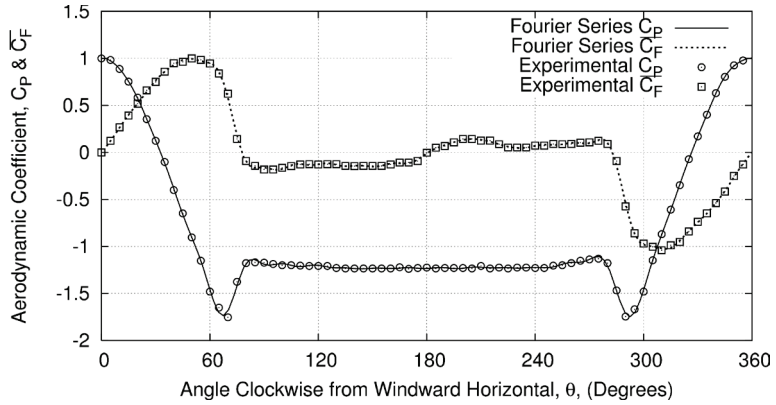

Figure 10. Numerical prediction of the temporal evolution of film thickness under shear and surface tension effects only.

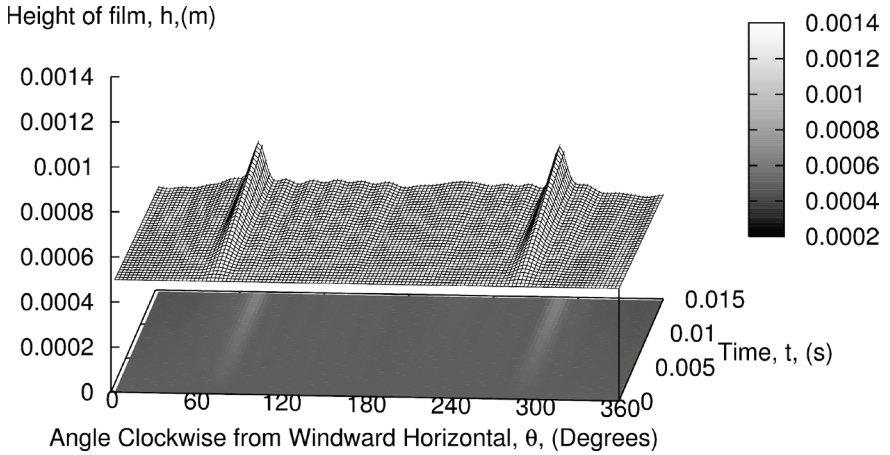

Figure 11. Comparison of current predictions of film thickness with results from Lemaitre *et al* (2007) : Film thickness at time t = 6.9 × 10^{-3} s under shear and surface tension effects only (flow from left).

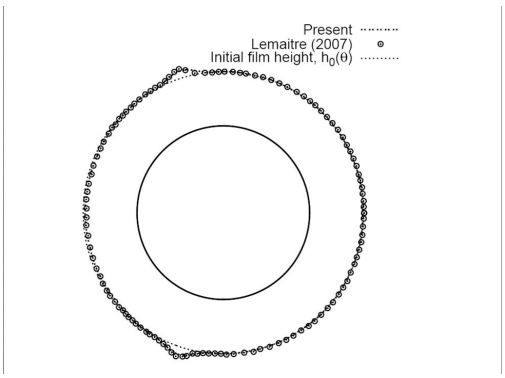

Figure 12. Numerical prediction of the temporal evolution of film thickness under pressure and surface tension effects only.

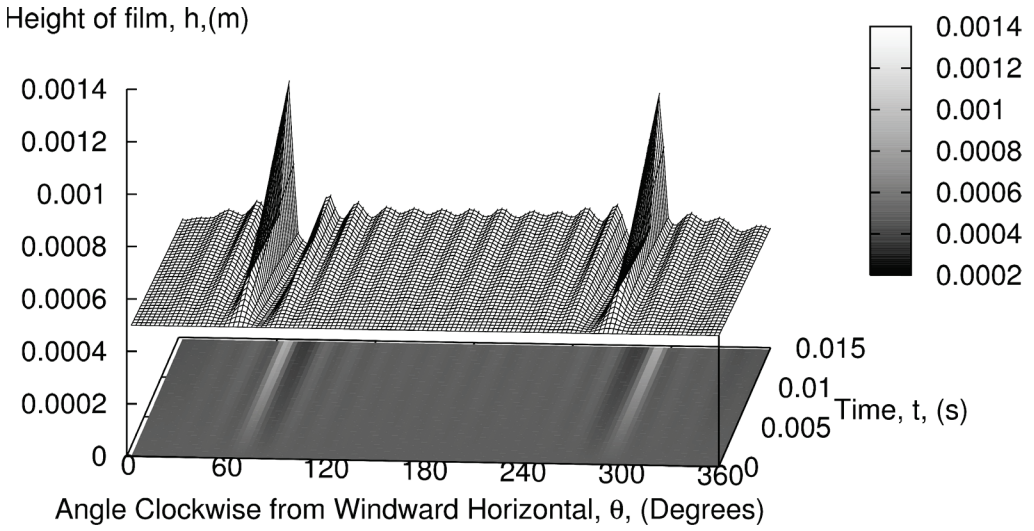

Figure 13. Comparison of predicted film thickness (100 × actual) for shear and surface tension loading with pressure and surface tension loading at time $t = 6.9 \times 10^{-3}$ s (flow from left).

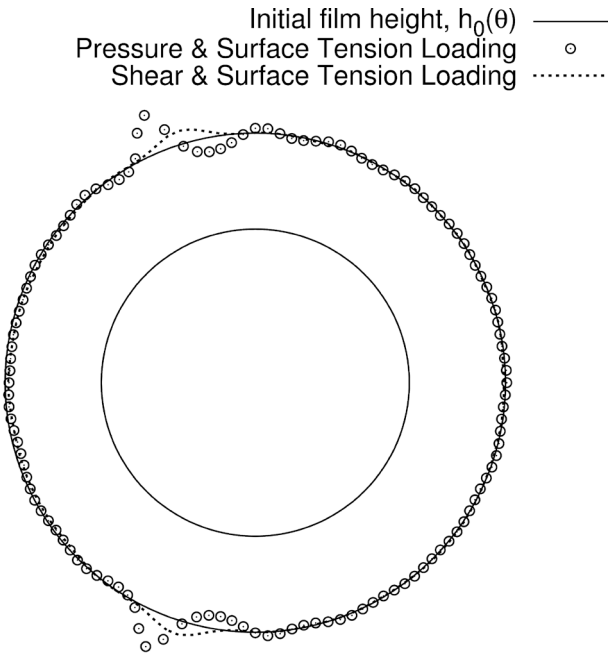

Figure 14. Numerical prediction of temporal evolution of film thickness under full loading conditions.

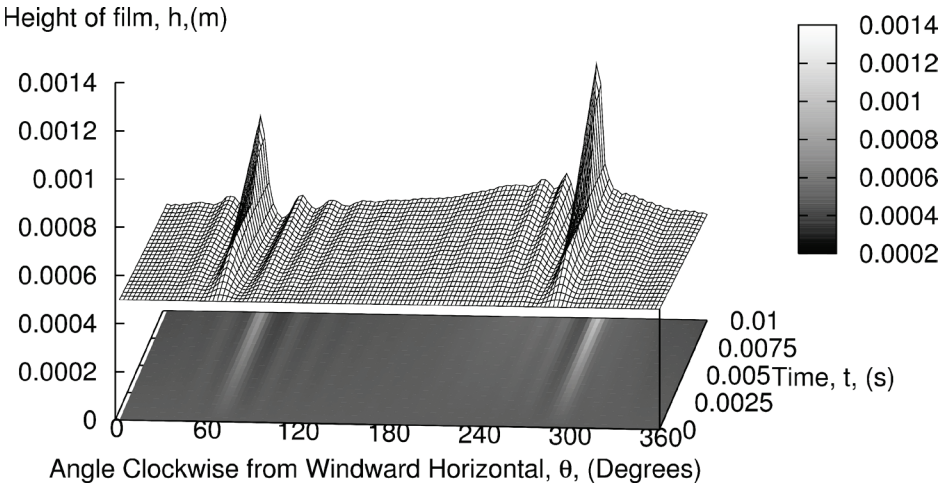

Figure 15. Evolution and growth of rivulet using the coupled model (non-dimensional time defined as $t^* = tU/D$).

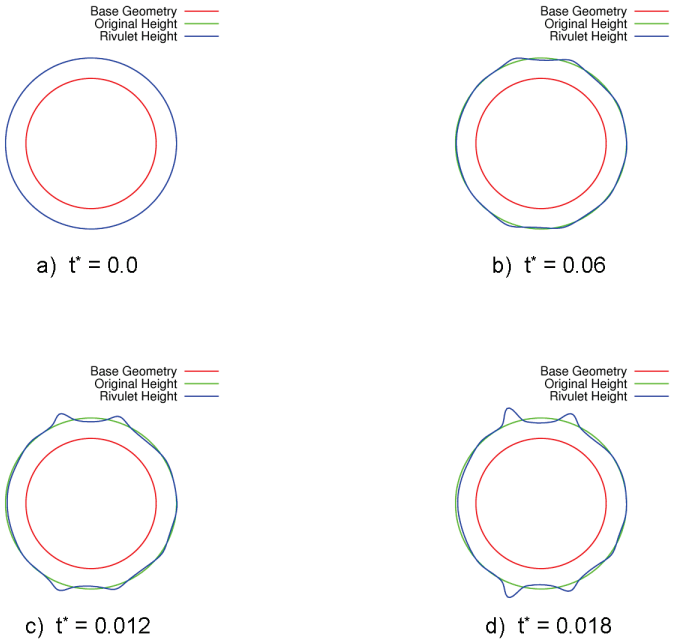

Table 1. Mean wind speed ranges reported for RWIV from full scale observations and wind tunnel investigations.

Bridge / Wind Tunnel	Wind-speed Range
Meiko-Nishi West Bridge (Hikami and Shiraishi, 1998)	7 to 14m/s
Erasmus Bridge (Geurts *et al*, 1998)	14m/s
Fred Hartman Bridge (Zuo *et al*, 2008)	5 to 15m/s
Dongting Lake Bridge (Ni *et al*, 2007)	6 to 14m/s
Three Bridges (Matsumoto *et al*, 1995)	6 to 17m/s
Wind Tunnel (Flamand, 1995)	7 to 12m/s
Wind Tunnel (Gu *et al*, 2002)	12 to 17m/s
Wind Tunnel (Cosentino *et al*, 2003)	7 to 12m/s

Table 2. Values of the standard parameters used in the numerical calculations.

Parameter	Values
Cylinder radius, R	0.08 m
Initial film thickness, h_0	5×10^{-4} m
Gravity, g	9.806 m/s^2
Density of water, ρ	1000 kg/m^3
Dynamic viscosity of water, μ	1.002×10^{-3} Ns/m
Surface tension of water, γ	72×10^{-3} N/m